Plasma Sources Science and Technology

PAPER

New insights into the lightning discharge processes

To cite this article: V A Rakov *et al* 2022 *Plasma Sources Sci. Technol.* **31** 104005

View the article online for updates and enhancements.

This content was downloaded from IP address 128.227.222.91 on 08/11/2022 at 18:28

IOP Publishing Plasma Sources Science and Technology
Plasma Sources Sci. Technol. 31 (2022) 104005 (17pp) https://doi.org/10.1088/1361-6595/ac9330

New insights into the lightning discharge processes

V A Rakov[1,*], M D Tran[1], Y Zhu[2], Z Ding[1], A F R Leal[3,4], I Kereszy[1,5] and S Chen[1]

[1] Department of Electrical and Computer Engineering, University of Florida, Gainesville, FL, United States of America
[2] Earth System Science Center, University of Alabama in Huntsville, Huntsville, AL, United States of America
[3] Department of Physics and Langmuir Laboratory, New Mexico Institute of Mining and Technology, Socorro, NM, United States of America
[4] Graduate Program in Electrical Engineering, Federal University of Pará, Belem, Brazil
[5] Department of Physics, University of Florida, Gainesville, FL, United States of America

E-mail: rakov@ufl.edu

Received 11 May 2022, revised 4 July 2022
Accepted for publication 20 September 2022
Published 31 October 2022

Abstract

This review covers selected results of recent observations of lightning discharges performed across the entire electromagnetic spectrum (radiofrequency, optical, and energetic radiation) at the Lightning Observatory in Gainesville, Florida. The most important results include (a) characterization of the preliminary-breakdown, stepped-leader, and return-stroke processes in high-intensity ($\geqslant$50 kA) negative lightning discharges, (b) the first high-speed video images of bidirectional leader that made contact with the ground and produced a return stroke, (c) discovery of negative stepped leader branches colliding with the lateral surface of neighboring branches of the same leader, (d) new data on the occurrence context and properties of compact intracloud discharges, and (e) observation of a terrestrial gamma-ray flash that occurred during a bipolar cloud-to-ground lightning discharge. The results serve to improve our understanding of the physics of lightning with important implications for lightning modeling, lightning protection, and high-energy atmospheric physics studies.

Keywords: lightning, leader, return stroke, compact intracloud discharge, terrestrial gamma-ray flash

(Some figures may appear in colour only in the online journal)

1. Introduction and overview of LOG setup

In this paper, we review several topics recently studied at the Lightning Observatory in Gainesville (LOG), Florida. The LOG includes a glass cupola on the roof of a five-story building providing over a 180° unobstructed view of the horizon. The cupola houses digitizing oscilloscopes, computers, and high-speed video cameras (operating in IR, visible, and UV ranges), with the various sensors and associated electronics being located nearby on the roof. The sensors currently include electric field (wideband and VHF) antennas, electric field derivative (dE/dt) antennas, magnetic field derivative (dB/dt) antennas, and an x-ray/gamma-ray detector (there is also a portable gamma-ray detector inside the cupola). Signals from the sensors on the roof are relayed by fiber-optic links or coaxial cables to the glass cupola, where they are recorded. All records are GPS time stamped. An overview and photographs of LOG are shown in figure 1. Multiple electric field and magnetic field sensors provide flexibility in running simultaneous measurements with different settings for the gain and instrumental decay time constant. NLDN (US National Lightning Detection Network) data are used to determine the distances to lightning channels and obtain estimates of peak

* Author to whom any correspondence should be addressed.

 © 2022 IOP Publishing Ltd Printed in the UK

current. In its present configuration, LOG allows us to perform observations of lightning across the entire electromagnetic spectrum covering the radiofrequency, optical (including IR and UV), and energetic radiation ranges. More information on LOG setup and characteristics of individual instruments/systems can be found in review papers by Rakov *et al* (2014, 2018).

The following selected topics recently studied at LOG are reviewed in this paper:

- Preliminary-breakdown (PB), stepped-leader, and return-stroke (RS) processes in high-intensity negative lightning discharges
- Bidirectional leader making connection to the ground and producing a RS
- Collisions of negative stepped leader branches
- Compact intracloud discharges (CIDs) and initiation of full-fledged lightning flashes
- Terrestrial gamma-ray flashes (TGFs)

2. PB, stepped-leader, and RS processes in high-intensity negative lightning discharges

The overall negative cloud-to-ground lightning discharge, often labeled −CG, consists of typically three to five component strokes or just strokes (Rakov and Uman 2003, chapter 4). Each stroke is composed of a downward moving leader and an upward moving RS. A leader initiating the first stroke in a flash exhibits stepping and is preceded by the initial or PB, which can be defined as the in-cloud process that initiates or leads to the initiation of the downward moving negative stepped leader. The PB involves the formation of a single channel or a sequence of channels. In the latter case, they extend in seemingly random directions from the cloud charge source with one of these channels evolving into the stepped leader which bridges the cloud charge source and the ground.

The PB process in ground flashes often produces a train of relatively large microsecond-scale electric field pulses. An example of pronounced PB pulse train in a multiple-stroke −CG is shown in figure 2. The time interval between the pulse train and the RS waveform is typically a few tens of milliseconds. The electric field amplitude of the PB pulses can be comparable to or even exceed that of the corresponding first RS pulse.

Using an automated data processing algorithm, Zhu *et al* (2016) have examined the characteristics of PB pulse trains and the following first RSs in −CGs in Florida. Out of 5498 flashes within 50 to 500 km of LOG, 3496 (64%) had PB pulse trains that were detected by the automated algorithm. For the 3077 flashes with one detectable PB pulse train and relatively high (⩾50 kA) first-stroke peak current, the arithmetic (geometric) mean values of peak current, PB pulse train duration, PB–RS interval, and PB/RS pulse peak ratio were 134 (122) kA, 2.7 (2.2) ms, 8.8 (7.5) ms, and 0.15 (0.13), respectively. The PB–RS interval was found to decrease with increasing NLDN-reported first-stroke peak current (see figures 3(a) and (b)), with the corresponding Spearman correlation coefficient being −0.80 (statistically significant at the 99.9% confidence level), and the strong correlation was also found in later studies by Nag and Cummins (2017) and Shi *et al* (2019).

Presented in table 1 are nine Florida negative flashes with short PB–RS intervals, examined by Zhu *et al* (2014), all of which exhibited high (AM = 131 kA) NLDN-reported RS peak currents. For five of the nine events, the corresponding lightning mapping array (LMA) data were available, which showed that the first LMA source heights ranged from 4.8 to 6 km. Based on these observed flash initiation heights and corresponding PB–RS intervals (stepped leader durations), Zhu *et al* (2014) estimated the geometric mean 1D stepped-leader speed to be 1.21×10^6 m s^{-1}. This speed value (although an underestimate of the actual, 3D, speed) is almost an order of magnitude higher than 2×10^5 m s^{-1} thought (e.g., Rakov and Uman (2003), chapter 4) to be typical for negative stepped leaders. Thus, the strong correlation seen in figures 3(a) and (b) suggests that negative flashes with faster stepped leaders tend to have higher first RS peak currents. On the other hand, Campos *et al* (2014) found no relation between the negative stepped leader speed and the corresponding RS peak current, although the number of events with peak current ⩾50 kA in their study was small (only 4).

As seen in figures 3(c) and (d), the largest range-normalized PB pulse peak exhibits statistically significant positive correlation with the RS peak current, with Spearman correlation coefficient being 0.48 (statistically significant at the 99.9% confidence level). Thus, it appears that the high-intensity (⩾50 kA) negative lightning discharges are characterized by both shorter (and, by inference, faster) stepped leaders and more pronounced (larger-amplitude) PB pulse trains.

PB is one of the least understood lightning processes. While it is logical to expect a faster leader to be followed by a more intense RS, it is not clear why the RS intensity is correlated with the intensity of PB which is an in-cloud process. Nag and Rakov (2016) found, via modeling, that peak currents associated with PB pulses are comparable to RS peak currents; that is, are of the order of tens of kiloamperes or more. Nag and Rakov (2009) and Kolmašova *et al* (2014) suggested that unusually fast stepped leaders are produced by unusually strong negative in-cloud charge sources. A faster stepped leader is likely to be associated with a higher leader tip potential, the latter being correlated with the prospective RS peak current and charge transfer. The events with short PB–RS intervals (fast leaders) were found by Kotovsky *et al* (2016) to be associated with long-lasting disturbances in the upper mesosphere and lower ionosphere. Additionally, PB or PB-type pulses were reported to produce TGFs recorded at ground level in Utah and Japan, although all TGFs observed at ground level in Florida were associated with processes other than the PB process (see section 6 of this paper). Clearly, further research of the PB process and its relation to other lightning processes is needed.

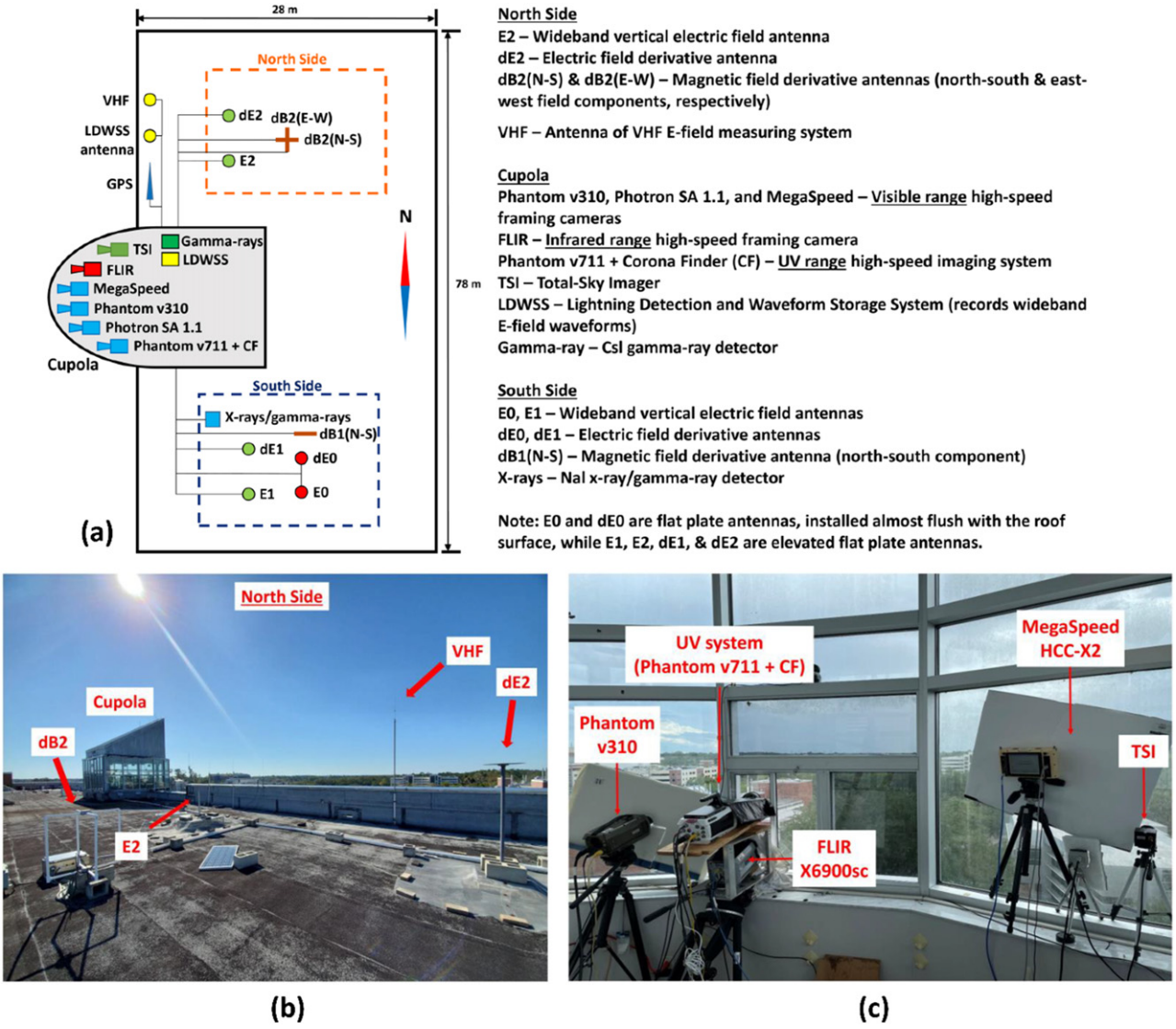

Figure 1. LOG, Florida. (a) Schematic overview, (b) photograph of the cupola (facing west) and various sensors installed on the roof, (c) photograph of the high-speed framing cameras installed inside the cupola. LDWSS and TSI were installed at LOG as part of collaboration with Adonis Leal (Federal University of Para, Brazil) and Weitao Lyu (Chinese Academy of Meteorological Sciences), respectively. The CsI gamma-ray detector was provided by Teruaki Enoto (RIKEN) and Yuuki Wada (Osaka University, Japan).

3. Bidirectional leader making connection to the ground and producing a RS

Tran and Rakov (2016) have optically imaged, for the first time, the entire evolution of a lightning bidirectional leader (see figures 4(a) and (b)), one end of which contacted the ground and produced a 36-kA RS. The bidirectional leader developed during the late stage of a cloud discharge and initiated in a decayed (not luminous for at least 43 ms) channel of that cloud discharge. The leader extended bidirectionally in virgin air for at least 12 ms with both ends branching. After turning toward ground, its negative end exhibited features characteristic of PB and stepped leader of first negative cloud-to-ground strokes, while the positive end (usually hidden inside the cloud) most of the time appeared to be inactive or showed intermittent luminosity enhancements. The bidirectional leader connected, via its positive end, to another bidirectional leader (floating channel) to form a larger bidirectional leader, whose negative end attached to the ground.

In order to examine electrical parameters of the bidirectional leader, a simple electrostatic model was applied to the time interval between −11.1 and −2.7 ms ($t = 0$ corresponds to the RS onset), during which the positive end could be reasonably well tracked. The channel (including branches) was represented by three straight sections, top horizontal, middle tilted, and bottom vertical (see figure 4(d)). The following assumptions were made. First, the neutral point (marked in figure 4) was stationary. Second, the line charge density along either positive or negative channel increased linearly from the neutral point (where it is zero) toward the far end. Third, the negative end extended at a variable speed estimated from the high-speed video images and with a constant charge density slope, while the positive end had a constant spatial extent

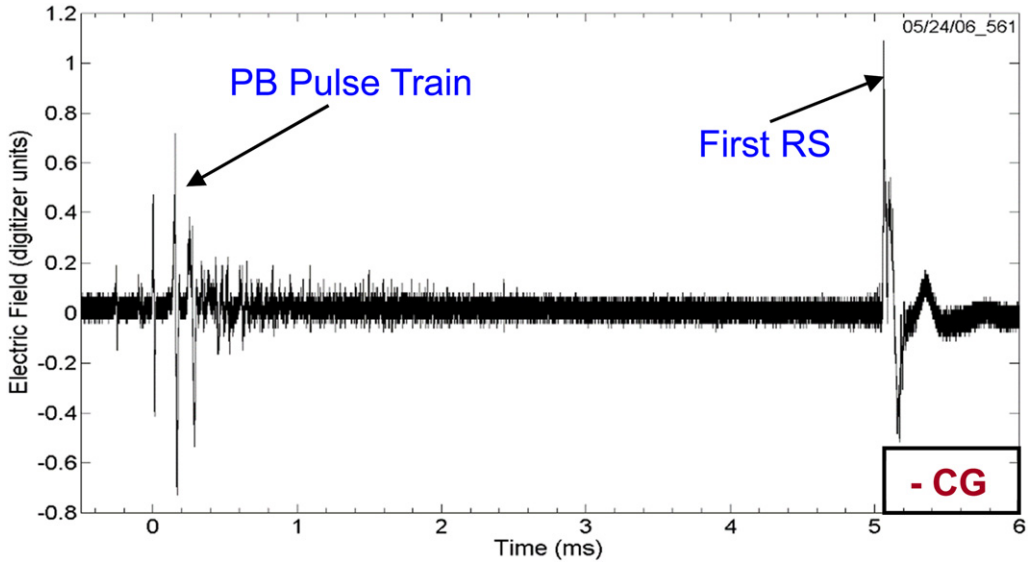

Figure 2. Electric field waveform of the first RS in a multiple-stroke negative CG flash (recorded at LOG) preceded by a PB pulse train. Time interval between the PB pulse train and the RS corresponds to the leader duration (in this case about 5 ms, smaller than the typical value). Reproduced with permission from [Nag, A., and V. A. Rakov (2008)]. © 2008. American Geophysical Union. All Rights Reserved.

(compare figures 4(a) and (b)) and a charge density slope increasing with time (to satisfy the principle of conservation of charge). It is likely that the positive-end charge was leaking into the surrounding air via corona discharge on the lateral surface of the channel and via corona streamers at the positive leader extremity. The negative charge density slope (3.7×10^{-7} C m^{-2}) was selected to match the net leader electric field change from -11.1 to -2.7 ms (94 V m^{-1} measured at LOG, 8.4 km from the lightning channel termination on ground). The net charge on the bidirectional leader channel was zero at all times. More details are found in Tran and Rakov (2016), (supporting information).

The line charge density as a function of distance from the neutral point at different instants of time is shown in figure 5. At -2.7 ms, the maximum magnitudes of charge density (at the extremity) of negative and positive leaders were found to be 1.6 and 5.5 mC m^{-1}, respectively. The charge transfer between -11.1 and -2.7 ms was 3.3 C, and the corresponding average current was 393 A. It was also found that uncertainties in the height of the horizontal channel section and in the location of the neutral point did not significantly affect the computed charge transfer value. If the slope of negative charge density is assumed to remain the same until the leader attachment to ground and the increase of positive end length due to connection to another floating channel is neglected, the total charge transfer Q will be 5.6 C. This is the charge deposited on the negative part of the bidirectional leader. If we assume that the charge neutralized by the RS is equal to that deposited on the negative part of bidirectional-leader channel, then according to the empirical formula relating the impulse charge transfer to the RS peak current, $I = 10.6Q^{0.7}$ (Berger 1972), the corresponding peak current will be 35 kA. The latter value is close to 36 kA reported by the NLDN for the RS initiated by the modeled bidirectional leader.

For comparison, if the positive part of the bidirectional leader were approximated by a time-varying point charge, the charge transfer and average current between -11.1 and -2.7 ms would be 3.0 C and 352 A, respectively. If, additionally, the negative end were assumed to be uniformly charged, the corresponding charge and current values would be 3.6 C and 429 A. All the values predicted by the simpler models (often used for computing leader electric fields at the ground surface) are within 10% or so of their counterparts predicted by the more elaborate model presented in figure 4.

To the best of our knowledge, this is the first detailed analysis of electrical parameters of $-$CG bidirectional leader constrained by high-speed optical images and electric field records.

4. Collisions of negative stepped leader branches

In order to demonstrate the generally unexpected phenomenon of collision of adjacent branches of the same leader, we present data for two downward negative stepped leaders that terminated on ground (or on insignificant protrusions above ground) at distances of 1.1 km (Flash Z1875) and 2.5 km (Flash Z1802) from LOG. Flash Z1875 had one stroke and Flash Z1802 had three strokes with only the first stroke being considered here. The stepped leaders presented here were imaged when they were at altitudes of some hundreds of meters above ground and within 1 ms prior to the RS onset. The leaders were heavily branched and each of them exhibited at least some tens of active tips at its lower extremity within the field-of-view (FOV) of the camera. We present results for Flash Z1875 first because they are more informative, in part due to this flash being closer to LOG than Flash Z1802. Flash Z1802 was recorded by the MegaSpeed, Phantom, and FLIR cameras (see figure 1), while Flash Z1875 only by the Phantom camera. MegaSpeed camera records are not shown in this paper.

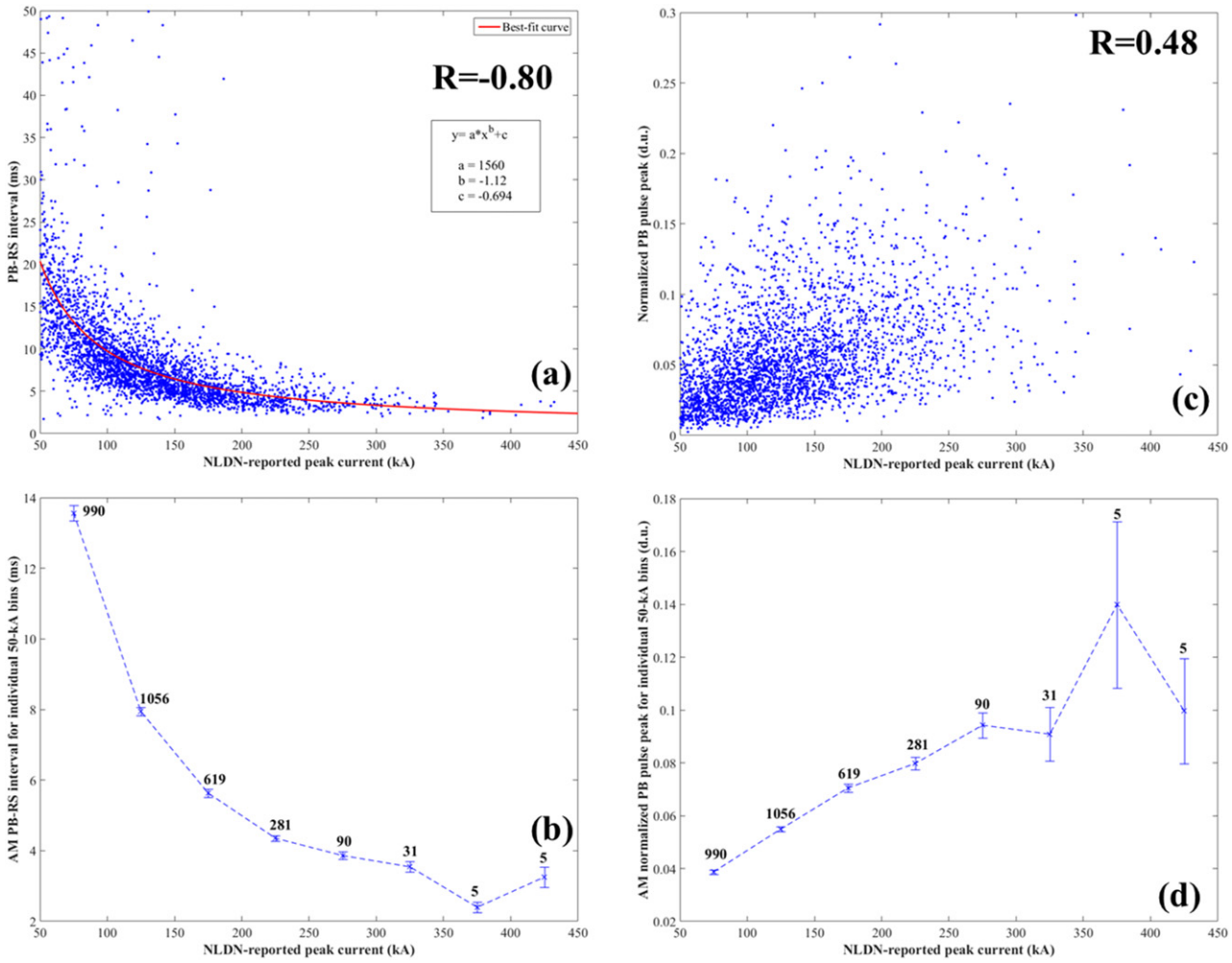

Figure 3. (a) Scatterplot of PB–RS interval versus NLDN–reported RS peak current, with the best-fit curve, $y = 1560x^{-1.12} - 0.694$, being shown by red line; (b) AM values of PB–RS interval for individual 50 kA bins versus NLDN–reported RS peak current; (c) scatterplot of the peak of the largest PB pulse normalized to 100 km (in digitizer units) versus NLDN–reported RS peak current; (d) AM values of normalized PB pulse peak for individual 50 kA bins versus NLDN–reported RS peak current. In (a) and (c), R is the Spearman correlation coefficient. In (b) and (d), the standard errors in mean values are shown by vertical bars and the corresponding sample sizes are given above them. Reproduced from [Zhu, Y., V.A. Rakov, and M.D. Tran (2016)]. CC BY 4.0.

Figure 6(a) shows a composite image of 60 inverted Phantom frames (pixel size = 2.2 m × 2.2 m) of Flash Z1875, from the frame in which the leader of stroke 1 first entered the FOV to the frame immediately preceding the RS frame. Two overlapping yellow-dotted boxes in figure 6(a) mark the regions for which individual frames are shown in figures 6(b) and (c). Similarly, figure 7(a) shows a composite image of 172 inverted Phantom frames (pixel size = 4.7 m × 4.7 m) of the leader stage of stroke 1 of Flash Z1802. The blue-dotted box in figure 7(a) marks the region for which individual frames are shown in figure 7(c). Figure 7(b) shows a single 1-ms FLIR frame of stroke 1 of Flash Z1802 including the late stage of leader and the RS. The white-dotted box in figure 7(b) marks the region for which two individual frames are shown in figure 7(d). Two collisions are seen in Flash Z1875 (figure 6) and one in Flash Z1802 (figure 7). The altitudes of collisions were between 370 m and 560 m above ground level (AGL). The process of collision usually involves two leader branches, which in the following we refer to as the leading branch (LB) and the chasing branch (CB).

Flash Z1875. In figure 6(b), the CB enters the FOV in frame −11 and the LB is first detectable in frame −10. The speeds of both the CB and the LB are specified on the right-hand side of each frame. The CB propagated more or less downward, while the LB extended mostly horizontally. Both of them moved at normal speeds of the negative stepped leader, although the LB was always faster. The LB bifurcated in frame −9, with the upper sub-branch coming in contact with the CB via a faint (streamer) link in frame −8. The CB is clearly seen collided with the lateral surface of the LB behind its tip in frame −7. Note that the LB accelerated between frames −9 and −8, decelerated between frames −8 and −7, and again accelerated between frames −7 and −6 and between frames −6 and −5. The LB shows enhanced brightness (luminosity blooming) near the leader tip in frames −5 and −4 and branching in frame −3. The CB is seen connected to the LB in frames −7 to −5.

Table 1. Characteristics of −CGs with short PB–RS intervals. Adapted from Zhu *et al* (2014).

Flash ID	Time interval between PB and first RS, T_{PB-RS} (ms)	First RS peak current reported by NLDN (kA)	Inferred leader speed, v[a] (m s^{-1})
839	3.5	222	1.61×10^6
854	4.5	133	1.3×10^6
881	5.9	82	0.78×10^6
882	6.0	102	—
1138	4.4	129	—
1203	4.0	150	1.23×10^6
1204	3.6	172	1.28×10^6
1205	4.3	110	—
1215	5.0	128	—
GM	4.5	131	1.21×10^6

[a]Estimated as $v = H/T_{PB-RS}$, where H is the altitude of the first LMA source. This estimate is a lower bound because the actual (3D) channel length should be considerably larger than H. For five strokes with peak currents >100 kA, $v > 10^6$ m s^{-1}.

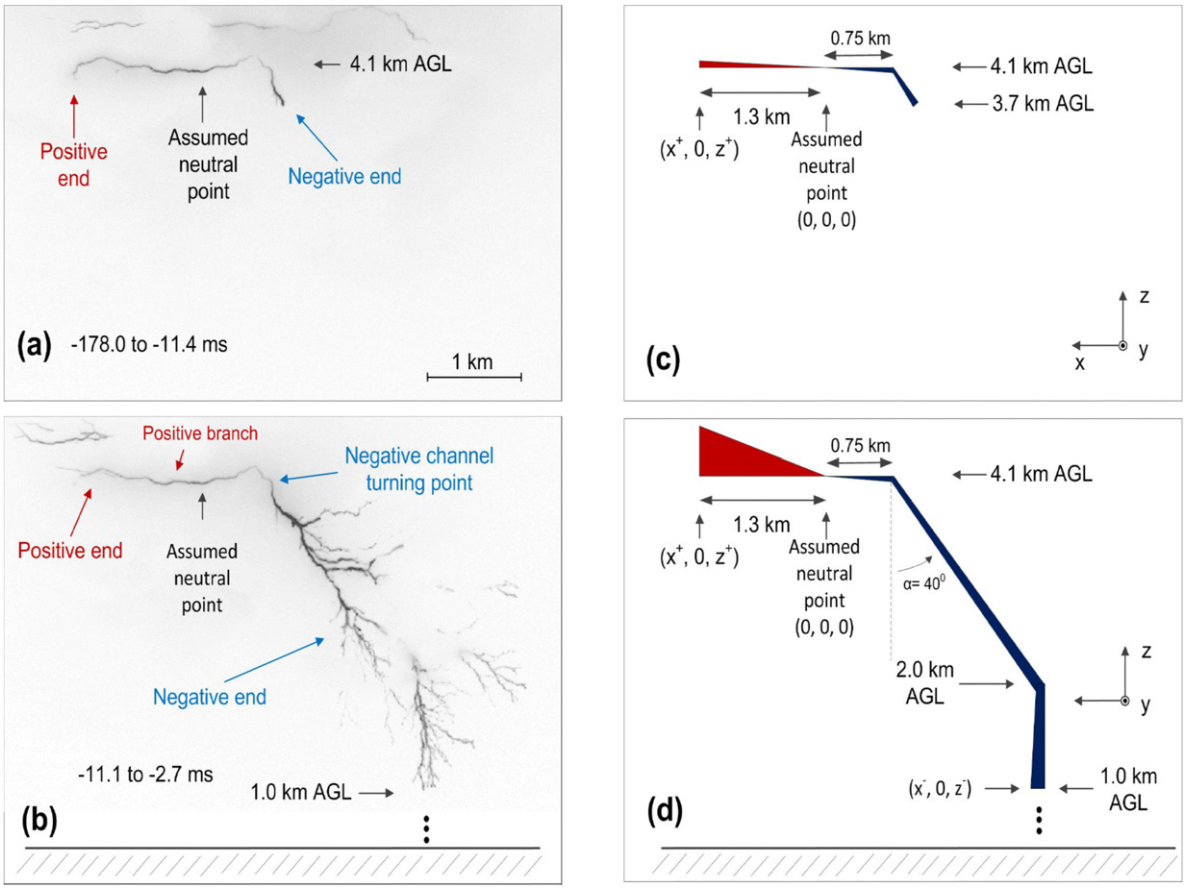

Figure 4. (a) Composite image of all frames of the bidirectional leader between −178 ms (the beginning of the high-speed video record) and −11.1 ms. (b) Composite image of all frames between −11.1 and −2.7 ms (frame −8.3 ms containing the transient event, which resulted in less than 5% difference in the total charge transfer, is excluded), showing the negative end descending from 4.1 to 1.0 km. (c) and (d) Geometries of the electrostatic model at −11.1 and −2.7 ms, respectively. The neutral point is assumed to be stationary between the rightmost positive branch labeled in (b) and the ground-bound turning point of the negative end. The line charge density is assumed to be linearly increasing from zero at the assumed neutral point to maxima at the extremities of the positive and negative leader channels. Reproduced from [Tran, M.D. and V.A. Rakov (2016)]. CC BY 4.0.

It became undetectable (apparently absorbed by the LB) in frame −4. Note a persistent brighter spot (BS), marked in frame −3, near the collision point. This BS remained detectable until the RS onset (frame 0, not shown in figure 6(b)). The CB apparently served to feed its negative charge into the LB.

Figure 6(c) shows an 80 m × 70 m region which overlaps the region shown in figure 6(b) (see figure 6(a)). One collision

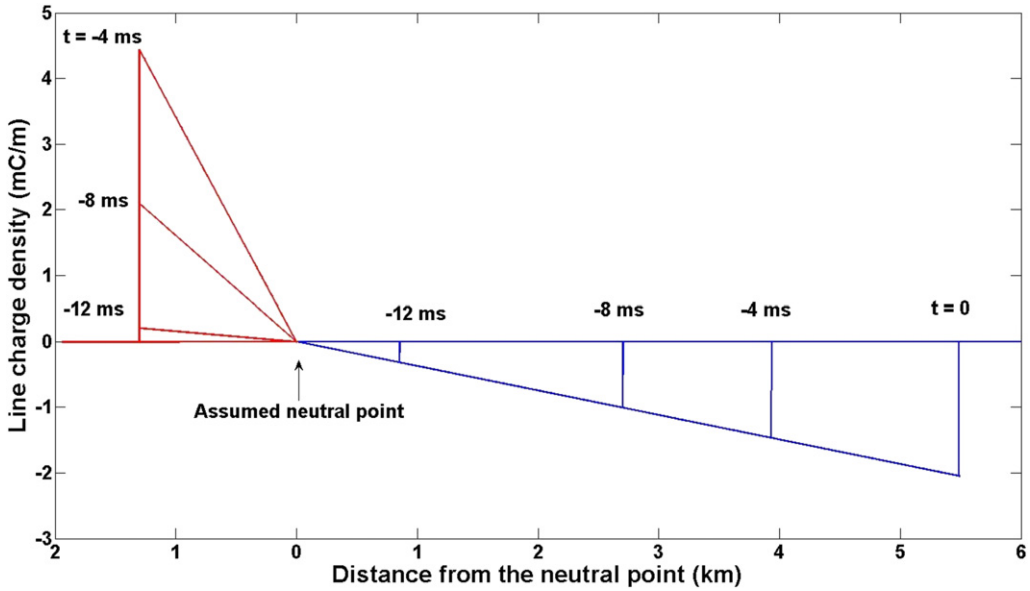

Figure 5. Line charge density vs unsigned distance from the neutral point. Red and blue lines correspond to the positive and negative parts of the bidirectional leader, respectively, at four (negative end) or three (positive end) instants of time, starting from −12 ms with a time step of 4 ms. The slope of line charge density for the negative end is constant, while for the positive end it increases to keep the net charge on the leader channel equal to zero at all times. The positive line charge density at $t = 0$ is not shown because at −2.4 ms the positive end connected to another floating channel of unknown length. Reproduced from [Tran, M.D. and V.A. Rakov (2016)]. CC BY 4.0

via a relatively faint (streamer) link is seen in frame −2 (it is also seen in figure 6(b)). Another possible collision is seen in frame −5. Also seen in figure 6(c) are frequent changes in branch direction (indicated by red arrows) and appearance/disappearance of relatively bright branches (compare, for example, frames −7 and −6), which, along with collisions, are indicative of a highly-structured and rapidly-changing local electric field pattern.

Flash Z1802. In figure 7(c), a clear collision is seen in frame −17 (where AP stands for the attachment point), with the collision scenario being generally similar to that seen in figure 6(b). The CB approached the LB from aside, collided with the lateral surface of the forked LB, and gradually faded away (became absorbed by the LB). Note that a streamer-like link was established between CB and LB in frame −18. Similar to figure 6(b), a BS near the AP is seen in frames −16 to −14. Attempted collision marked in frame −15 was identified via the reduced gap between the branches involved in frame −15 relative to preceding frame −16 and following frame −14.

Branch collisions described above are likely facilitated by the leader stepping process. Prior to each step, the leader channel is negatively charged, with the bulk of the charge being stored in the corona sheath surrounding the narrow hot core. When stepping occurs, positive charge is injected at the leader tip into the hot channel core in the form of an upward-traveling wave. This positive charge serves to partially neutralize the negating corona-sheath charge and, as a result, the wave magnitude is decreasing with height. After traveling over some hundreds of meters the positive charge wave runs out of steam (becomes absorbed in the negative corona sheath), and the channel that it just traversed becomes negative again. Everything in the above description is similar to the RS, except for the channel being not grounded and the magnitude of positive charge injected at the tip being small compared to the negative charge stored in the channel. Experimental evidence of upward-moving waves (mini RSs) in negative leaders is found in Wang *et al* (1999). Upward-moving positive charge waves were also reproduced in the numerical model of negative leader developed by Syssoev *et al* (2020). During the leader stepping process, the positive charge wave moving upward along the hot core can interact not only with the negative space charge stored in the surrounding corona sheath but also with downward-extending leader branches (carrying negative charge) that happen to be nearby. As a result, a negatively-charged branch tip can collide with the lateral surface of the adjacent (leading) branch of the same leader, as seen in figures 6 and 7, due to Coulomb attracting force of the step-related positive charge moving along the LB core. More details can be found in Ding and Rakov (2022).

5. CIDs and initiation of full-fledged lightning flashes

CIDs are mysterious lightning discharges inside the cloud that are characterized by short (usually shorter than 1 km) inferred channel lengths, very strong HF–VHF (3–300 MHz) radiation, and characteristic bipolar wideband electric field pulses (referred to as narrow bipolar pulses or NBPs) having a typical total width of 10–30 μs and large amplitudes that are comparable to those of pulses produced by RSs in cloud-to-ground discharges at similar distances. At short distances, electromagnetic signatures of CIDs can be dominated by the induction field component and, hence, are not necessarily

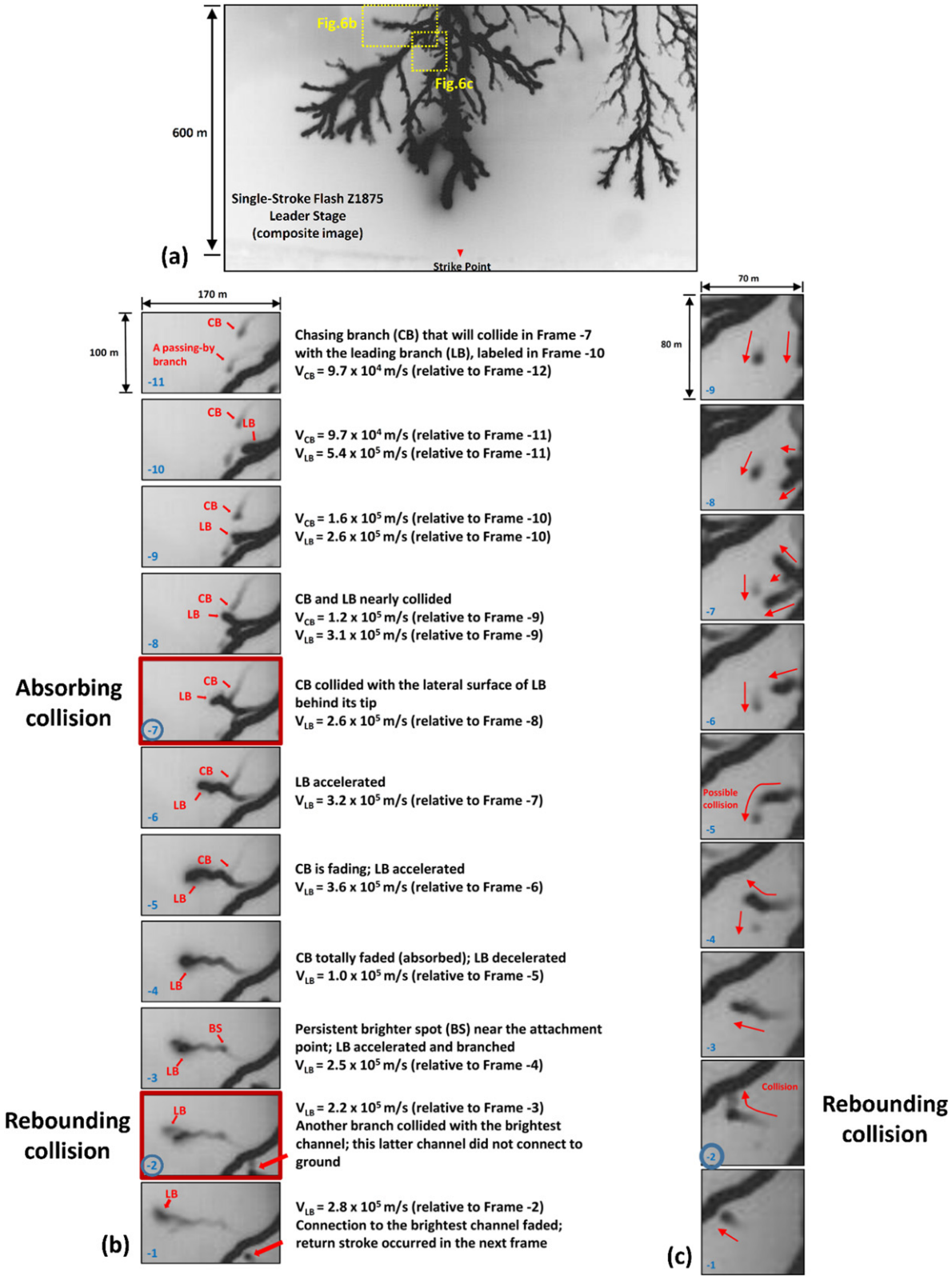

Figure 6. Flash Z1875. (a) Composite image of the negative stepped leader of single-stroke Flash Z1875. Yellow dotted boxes mark the regions for which consecutive 50 μs Phantom frames are shown in (b) and (c). Reproduced with permission from [Ding, Z., Rakov, V. A., Zhu, Y., Tran, M. D., Kostinskiy, A. Y., & Kereszy, I. (2021)]. © 2021. American Geophysical Union. All Rights Reserved.

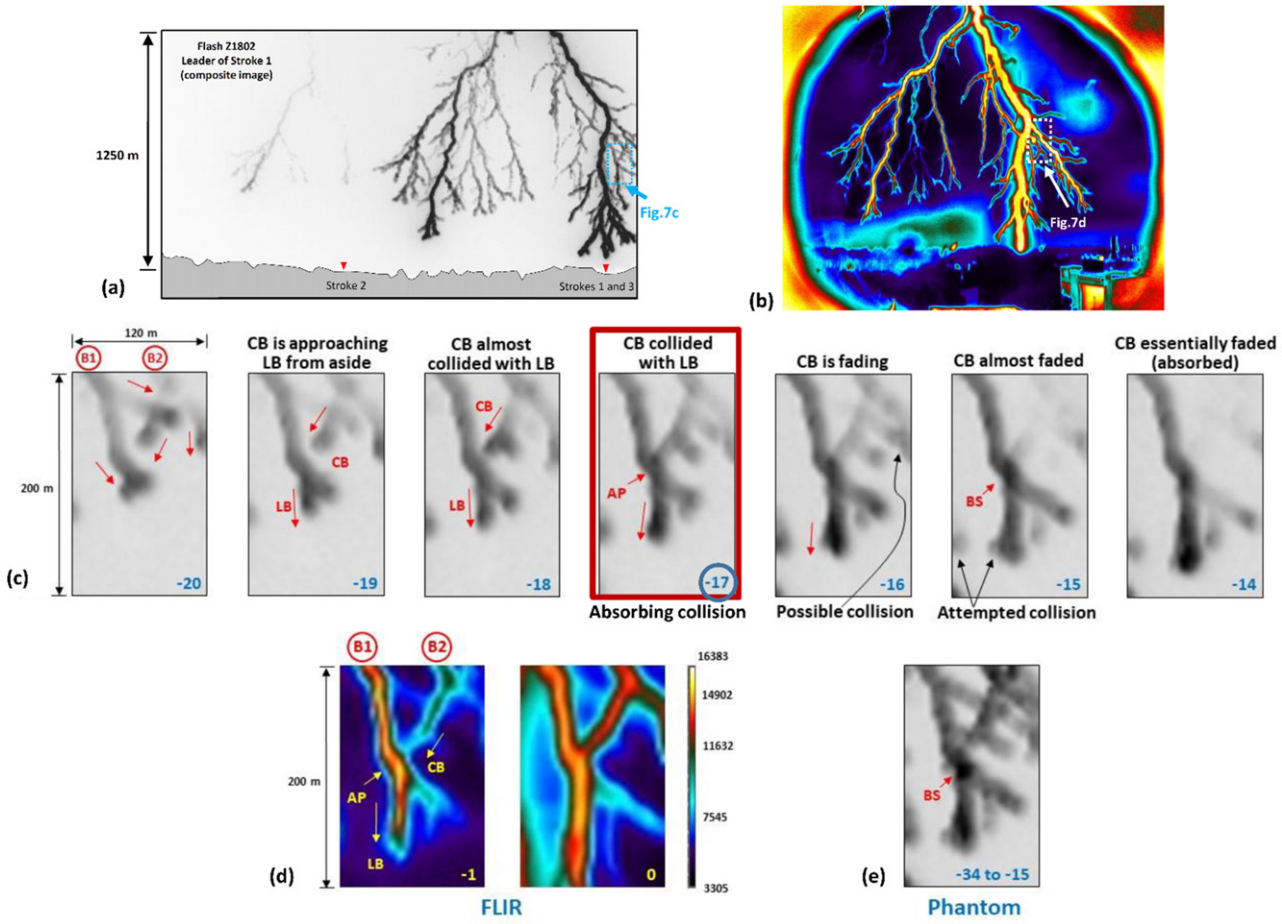

Figure 7. Flash Z1802. (a) Composite Phantom image of the negative stepped leader of stroke 1. Blue dotted box marks the region for which individual frames are shown in (c). (b) A single 1-ms FLIR frame of stroke 1 including the late stage of leader and the RS. White dotted box marks the region for which individual frames are shown in (d). (c) Seven consecutive 50-μs Phantom frames showing the dynamics of leader branches in blue-dotted box labeled '(c)' in (a). (d) Two consecutive 1-ms FLIR frames, where frame −1 is the last frame corresponding to the leader stage and frame 0 includes both the late stage of leader and the RS. (e) Composite Phantom image including 20 50-μs frames approximately corresponding to the 1-ms FLIR frame −1 shown in (d). Note a persistent BS near the attachment point in (e) (also marked in frame −15 in (c)). Reproduced with permission from [Ding, Z., Rakov, V. A., Zhu, Y., Tran, M. D., Kostinskiy, A. Y., & Kereszy, I. (2021)]. © 2021. American Geophysical Union. All Rights Reserved.

bipolar (e.g., Eack (2004), Karunarathne *et al* (2016)). CIDs are also known as narrow bipolar events. Most of CIDs occur between the main negative and main positive charge regions (lower-level CIDs), but some occur between the main positive and screening negative charge regions (upper-level CIDs), as illustrated in figure 8(a).

Observations of CIDs were first reported by Le Vine (1980). Since then, many researchers have been reporting this phenomenon from observations in different regions of the world including the United States (e.g., Willett *et al* (1989), Smith *et al* (1999), Nag *et al* (2010), Karunarathne *et al* (2015), Leal *et al* (2019)), Sri Lanka (e.g., Sharma *et al* (2008)), Malaysia (e.g., Azlinda Ahmad *et al* (2010)), China (e.g., Zhu *et al* (2010), Wu *et al* (2011, 2012), Liu *et al* (2012), Lü *et al* (2013)), and Japan (e.g., Wu *et al* (2013)). Perhaps the most puzzling feature of these mysterious lightning events is the fact that their VHF radiation (which is expected to be indicative of PB and leader processes creating a new lightning channel), and their wideband signature (which is indicative of a current wave propagating along the already existing channel) appear to be generated at the same time.

Compared to other forms of lightning, our understanding of the physics of CIDs is still poor. Cooray *et al* (2014) modeled the CID as one or more relativistic avalanches and related the well-known 'noisiness' of dE/dt waveforms produced by CIDs to multiple avalanche bursts. However, Rison *et al* (2016) argued that there is little or no evidence that energetic electron avalanches are involved in CIDs and proposed their own CID mechanism: extremely fast (3×10^7 to 10^8 m s^{-1}; Krehbiel *et al* 2018) positive breakdown occurring in virgin air and leaving behind no conducting channel. Tilles *et al* (2019) reported that a similarly fast breakdown of opposite (negative) polarity can also produce CIDs. Further, Huang *et al* (2021) identified a 'mixed fast breakdown' in which both positive and negative streamers propagate simultaneously from the initiation point. Attanasio *et al* (2021) introduced the concept of 'bidirectional fast breakdown' in which electric field enhancement ahead of the propagating fast breakdown of one polarity initiates a 'rebounding' fast breakdown of

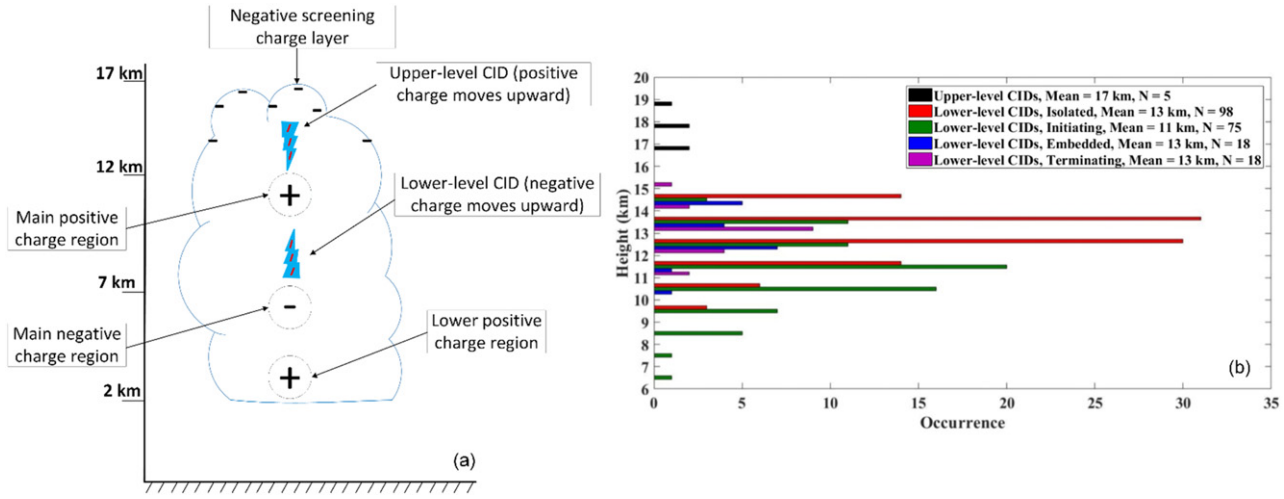

Figure 8. (a) Schematic representation of lower-level and upper-level CIDs; (b) CID heights for four categories of lower-level CID occurrence context (see figure 9) and for all categories of upper-level CID context combined, shown in 1-km bins. *N* is the sample size.Reproduced from [Leal, A. and V.A. Rakov (2019)]. CC BY 4.0.

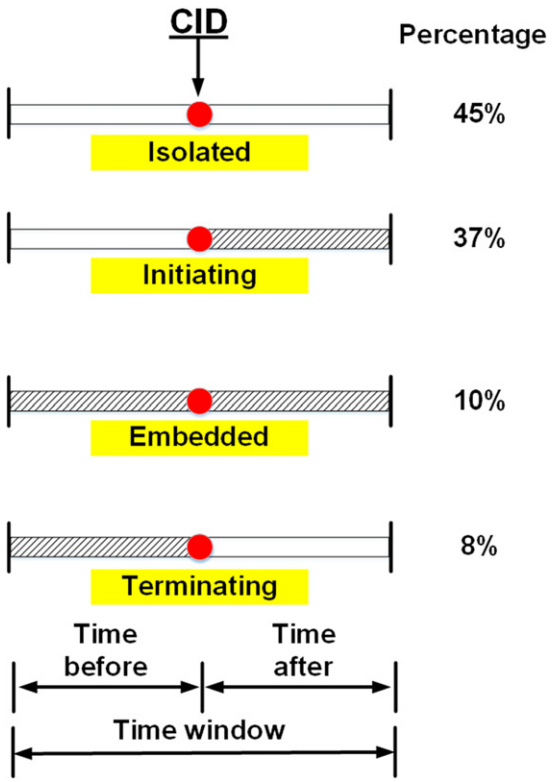

Figure 9. CID occurrence context. The red circle indicates the position of CID at the center of the time window and the shading indicates the occurrence of other lightning events (not CIDs). The percentages are given for the ±500 ms time window and 10 km search radius. Reproduced from [Leal, A. and V.A. Rakov (2019)]. CC BY 4.0.

opposite polarity. Nag and Rakov (2010a) observed periodic variations in their d*E*/d*t* records of CIDs and inferred that, from the electromagnetics point of view, the CID is essentially a bouncing-wave phenomenon. Putting aside the question of how the wave-guiding structure was created, they suggested that the process could be viewed as a long wave repeatedly folding on itself. Li *et al* (2022) proposed a 'rebounding wave' model of CID, which appears to be a variant of Nag and Rakov's (2010a) bouncing-wave model.

Leal *et al* (2019), who examined over 1000 CID electric field waveforms, found that more than half of them showed pronounced periodic variations (ringing) on the opposite-polarity overshoot of their bipolar electric field waveforms (two-thirds according to Karunarathne *et al* (2015)), which, as noted above, is indicative of a bouncing wave process. The period of variations suggests a wave propagation speed of the order of 10^8 m s^{-1} for the expected longitudinal dimension of CID of a few hundreds of meters. It is important to note that, as evidenced by the corresponding d*E*/d*t* records, the ringing occurs during the first half-cycle of the CID *E*-field waveform, not only during the slower opposite-polarity overshoot, where it is easier to detect (Nag and Rakov 2010a). Those observational facts suggest that the bouncing behavior is a fundamental property of CIDs.

Rison *et al* (2016) visualized their fast positive breakdown as a system of cold streamers extending over some hundreds of meters inside the cloud. However, it is difficult to imagine that a large streamer formation can remain essentially homogeneous during its lifetime of the order of 10 μs or so. Indeed, hot channel segments are likely to be created inside the streamer formation via the thermal ionizational instability (e.g., Raizer (1997), section 9.4, Raizer (2009), section 13.4) and redistribution of current within the overall streamer structure due to interaction of streamer branches with each other. The occurrence of such hot channel segments inside streamer formations on the time scale of the order of 1 μs was experimentally observed in laboratory by Kostinskiy *et al* (2015, 2022) and discussed in the context of lightning initiation by Kostinskiy *et al* (2020) and Iudin *et al* (2021). Further, there exists some observational evidence of hot channel segments associated with CIDs, which is reviewed next.

One of the main findings from the FORTE satellite mission is that CIDs produce 'little-to-no light output' (see Light

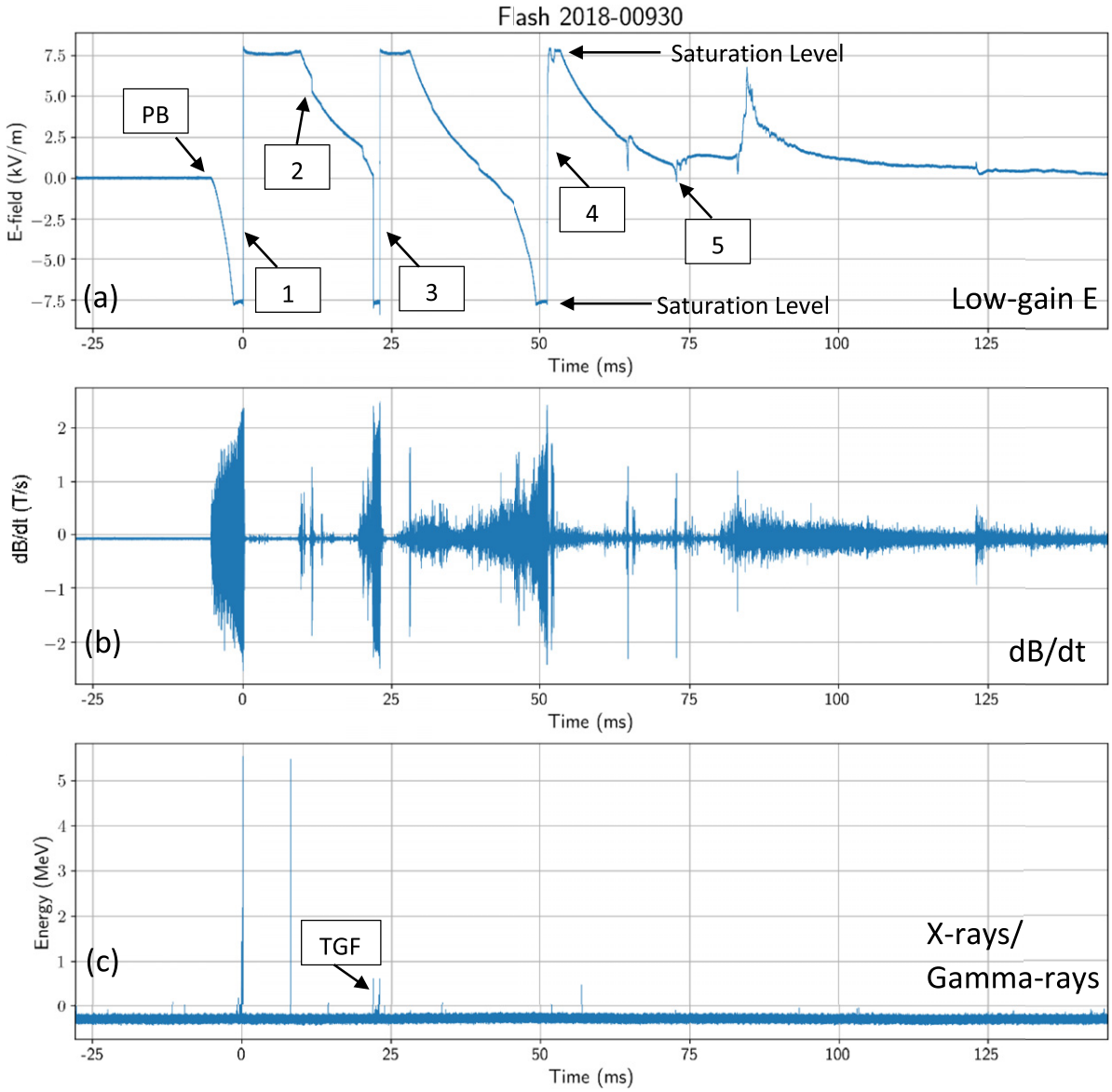

Figure 10. Overall records of (a) low-gain electric field ($\tau = 10$ ms), (b) magnetic field derivative (dB/dt), and (c) x-rays/gamma-rays for the five-stroke bipolar flash during which the TGF (marked in (c)) presented here was observed. In (a), the numbers indicate stroke order. No x-rays/gamma-rays were observed during the PB process. Records for strokes 1, 3, and 4 in all three panels are clipped due to measuring system saturation. Full time scale is 175 ms. $t = 0$ corresponds to the onset of the RS stage of stroke 1. Reproduced with permission from [Kereszy, I., V.A. Rakov, Z. Ding, and J.R. Dwyer (2022)]. © 2022. American Geophysical Union. All Rights Reserved.

(2020) and references therein). This was confirmed by ground-level observations of Jacobson *et al* (2013), (table 5), who reported that out of 193 lower-level CIDs (see figure 8(a)) only 2 (1%) were accompanied by optical (350–1100 nm) signals and none out of 24 upper-level CIDs did so. More recently, Stolzenburg *et al* (2021), (figures 5 and 11), from ultra-high speed (6.1 μs exposure time) video observations, reported on faint luminosity enhancements in the 350–1060 nm (with peak at 670 nm) range associated with two lower-level CIDs.

Significant new insights into optical emissions of CIDs have been made possible via spectral measurements by the ASIM installed on the International Space Station. It has been determined that CIDs emit strong signals at 337 nm, which is indicative of their primarily cold-streamer nature. However, Neubert *et al* (2021), (figure 3), also reported, for an upper-level CID (see figure 8(a)), a detectable signal at 777.4 nm, which is indicative of hot channels. In contrast, Soler *et al* (2020) and Li *et al* (2021) did not observe above-noise emissions at 777.4 nm in their ASIM records corresponding to lower-level and upper-level CIDs, respectively. Also, Liu *et al* (2021) found only 'weak or no detectable emissions at 777.4 nm' in the ASIM data corresponding to both upper-level and lower-level CIDs, although one lower-level CID was accompanied by detectable emission at 777.4 nm, which the authors attributed to 'some extra sferic-radiated activity' following the main pulse. More recently, Liu *et al* (2022), while reiterating on the streamer nature of CIDs, as evidenced by pronounced 337 nm emissions, also presented

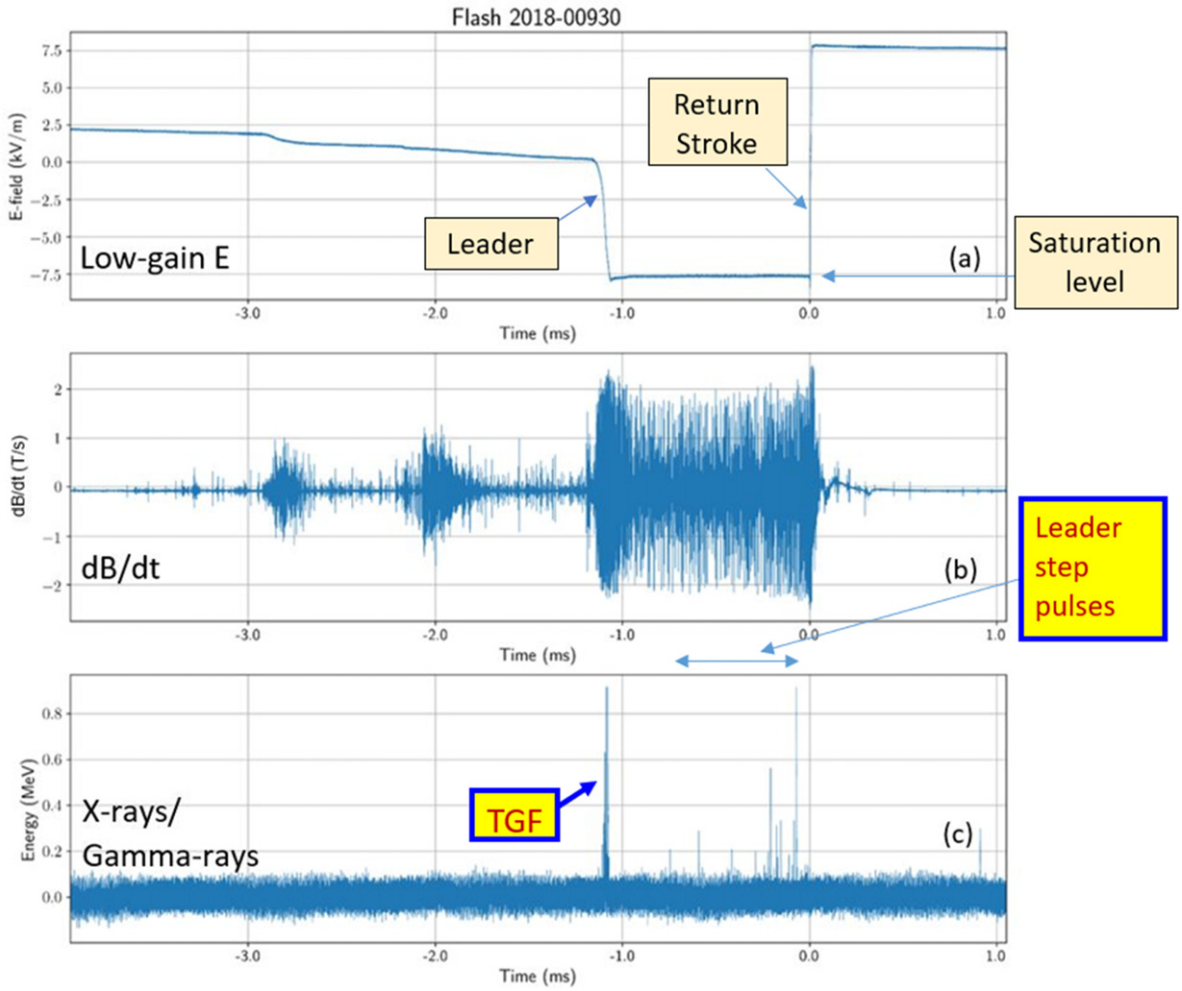

Figure 11. (a) Electric field waveform, (b) dB/dt waveform, (c) x-rays/gamma-rays for stroke 3 (negative; $r = 200$ m). TGF, marked in (c), and the corresponding E-field record are shown on an expanded time scale in figure 12 (dB/dt record is not shown there due to strong saturation). $t = 0$ corresponds to the onset of the RS stage of stroke 3. Full time scale is 5 ms. Reproduced with permission from [Kereszy, I., V.A. Rakov, Z. Ding, and J.R. Dwyer (2022)]. © 2022. American Geophysical Union. All Rights Reserved.

in their figure 2 a small 777.4 nm (hot-channel) signature of CID. Based on the above, we hypothesize that relatively small, and therefore often undetectable, hot channel segments can be formed inside the overall cold-streamer structure, as schematically shown by red dashes embedded in blue CID symbols in figure 8(a).

There is currently a debate on the role of CIDs in lightning initiation. According to Rison *et al* (2016), many or possibly all lightning flashes are initiated by fast positive breakdown, which, they suggest, is the unique physical process behind CIDs. Most lightning discharges, however, are known to be not preceded by a CID-like radiofrequency (RF) electromagnetic field signature (e.g., Nag *et al* (2009), Marshall *et al* (2019), Lyu *et al* (2019)). Different lightning initiation scenarios seem to be possible. According to Leal and Rakov (2019), only 37% of CIDs initiate full-fledged flashes and 63% do not, with 45% of CIDs being isolated, which is the most common CID occurrence context (see figure 9). CIDs initiating full-fledged flashes tend to occur at lower altitudes (mean = 11 km vs 13 km for other CID occurrence contexts; see figure 8(b)).

It appears that CIDs can initiate (or lead to the initiation of) the so-called transient luminous events developing from clouds toward the ionosphere, which include blue starters, blue jets, and gigantic jets. Specifically, lower-level CIDs (occurring between the main negative and main positive charge regions) were reported to precede gigantic jets by some hundreds of milliseconds (Krehbiel *et al* 2008, Lu *et al* 2011, Liu *et al* 2015). More recently, Chou *et al* (2018) observed six 'blue luminous events' that were accompanied by upper-level CIDs, occurring between the main positive and screening negative charge regions, at heights ranging from 16 to 18 km AGL. Similarly, Liu *et al* (2018) reported on six 'blue discharges' each occurring within 1 ms (their time uncertainty) after an upper-level CID occurring at a height in the 15 to 18 km range AGL. Interestingly, while upper-level CIDs appear to directly initiate upward-jet-type events, lower-level CIDs do so via normal ICs lasting some hundreds of milliseconds. Neubert *et al* (2021) suggested that microsecond-scale 'blue flashes' that have been observed at cloud tops (sometimes developing into upward extending blue events) from orbit are optical signatures of CIDs.

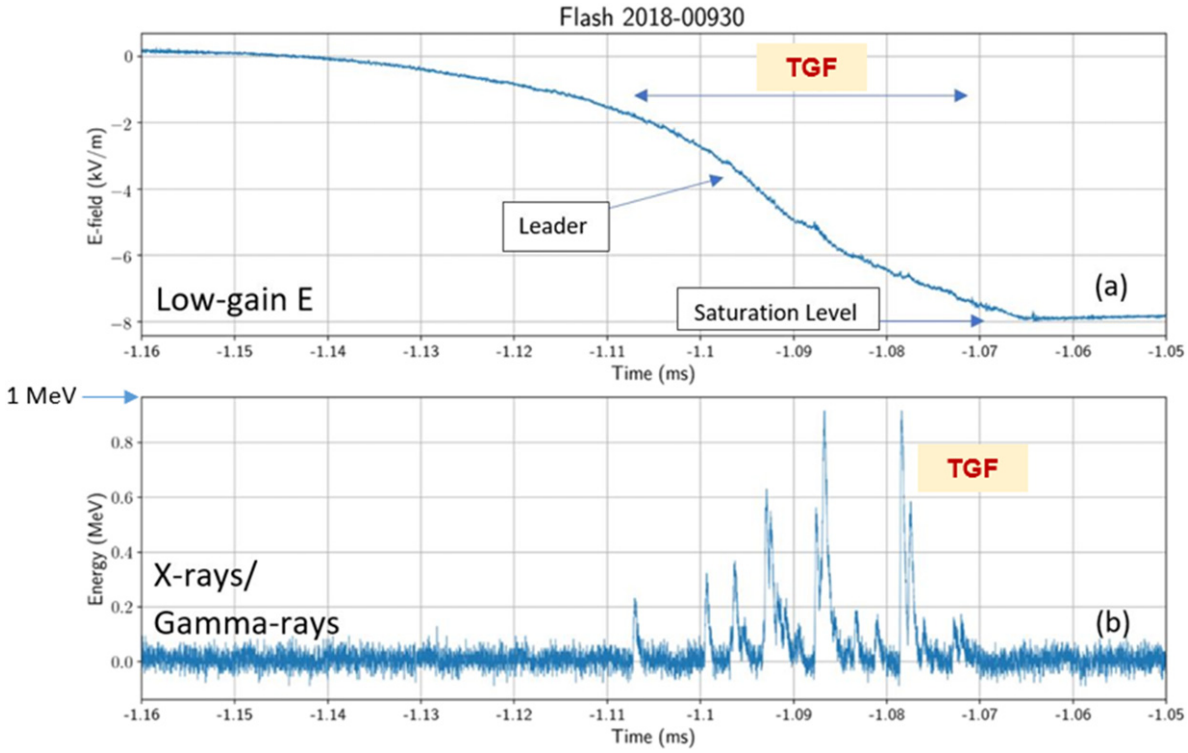

Figure 12. (a) Electric field waveform corresponding to the initial stage of the leader of stroke 3 (negative). (b) TGF inferred to be associated with an in-cloud part of stroke 3 (leader entering the decayed but still warm channel to ground created by stroke 2 (positive)). $t = 0$ corresponds to the onset of the RS stage of stroke 3. Full time scale is 110 μs. Reproduced with permission from [Kereszy, I., V.A. Rakov, Z. Ding, and J.R. Dwyer (2022)]. © 2022. American Geophysical Union. All Rights Reserved.

6. Terrestrial gamma-ray flashes

TGFs are defined here as bursts of gamma-rays less than 1 ms or so in duration, whose sources are located inside thunderclouds, at typical altitudes of several kilometers or more AGL. In contrast, x-rays/gamma-rays (in lightning research, the boundary between the two is usually placed at 1 MeV) are produced by all types of downward leaders when they come typically within a few hundreds of meters of the ground (e.g., Dwyer *et al* (2004a), Mallick *et al* (2012)). In either case, avalanches of runaway electrons experiencing deflection by the electric field of other charged particles (typically atomic nuclei) are involved. However, specific mechanisms/scenarios may differ, depending on the source of seed electrons, the magnitude and spatial extent of the electric field, and other factors. Energetic radiation associated with downward leaders in negative cloud-to-ground flashes (−CGs) is usually detected (and identified as such) at the ground within less than 1 ms of the RS onset (see, for example, figure 7 of Mallick *et al* (2012)). TGFs are mostly observed from space (e.g., Fishman *et al* (1994), Smith *et al* (2005), Briggs *et al* (2010), Neubert *et al* (2020)) and rarely seen at the ground.

Tran *et al* (2015) reported on a TGF observed in 2014 at LOG. It was associated with a single-stroke 224-kA −CG at a distance of 7.5 km from LOG. The TGF had a duration of 16 μs and was composed of six detectable photons, four of which were in the MeV-range. The corresponding RF electromagnetic field signatures were recorded at LOG and supplemented by field signatures at larger distances recorded by the NLDN and by the Earth Networks Total Lightning Network (ENTLN). The TGF occurred 202 μs after the RS onset and was accompanied by an electric field derivative (dE/dt) burst. The latter observation suggests that RREA or other relativistic process responsible for the TGF production and the low-energy streamer formation process responsible for the dE/dt burst can be taking place concurrently. Other ground-based TGF observations in Florida include three events recorded at Camp Blanding, two associated with rocket-and-wire triggered lightning (Dwyer *et al* 2004b, Hare *et al* 2016) and one with natural lightning (Dwyer *et al* 2012). All four previously reported events from Florida occurred in the presence of steady current carrying negative charge to ground, well after the flash initiation processes.

We now present in more detail the fifth (and most recent) Florida TGF, which was recorded at LOG in 2018 and occurred in a rather unusual context, between opposite polarity strokes of a bipolar cloud-to-ground lightning flash. Bipolar lightning discharges sequentially transfer to ground both positive and negative charges during the same flash (Rakov 2005). They constitute roughly 10% of the global lightning activity. The flash in question created a total of three channels to ground, the first one taken by stroke 1 only, the second one taken by strokes 2 and 3, and the third one by strokes 4 and 5. The overall E-field, dB/dt, and x-ray/gamma-ray records of the flash are shown in figure 10. The E-field records in this paper are shown using the atmospheric electricity sign convention

Table 2. Acceleration and multiplication of runaway electrons.

Process	Source of seed electrons	Air temperature (K)	Electric field[a](MV m^{-1})
Relativistic avalanches in cold air (cold runaway breakdown)	Two-step process starting with ambient distribution	300	$\gtrsim$30
Relativistic avalanches in cold air (RREA)	Cosmic-ray secondaries	300	~0.2
Relativistic avalanches in remnants of decayed channel	Ambient distribution	3000	$\gtrsim$3
Conventional (non-relativistic) avalanches in cold air	Ambient distribution	300	~3

[a]Approximate values at sea level.

(e.g., Rakov and Uman (2003), section 1.4.2), according to which the downward directed electric field or electric field change vector is assumed to be positive (negative RS field change deflects upward).

Data for stroke 3 (TGF producer) are shown in figures 11 and 12. According to the NLDN data, stroke 3 followed the remnants of the channel to ground created by stroke 2, about 200 m from LOG. This is confirmed by the <3 ms duration of the leader of stroke 3 (see figure 11), which is characteristic of a leader developing in previously created channel (leaders creating a new channel usually take tens of milliseconds to reach ground). We infer from the entirety of our data that the negative leader initiating stroke 3, while developing horizontally inside the cloud along the residual channel of stroke 1 passing over LOG, entered the remnants of the warmer channel to ground created by stroke 2 (about 200 m from LOG), where that negative leader produced the TGF seen in figures 11(c) and 12(b).

The TGF had a duration of 35 μs and consisted of 18 pulses with amplitudes ranging from 114 to 912 keV. For comparison, the TGF previously recorded with the same instrumentation at LOG (Tran *et al* 2015) contained pulses exceeding the detector saturation level of 5–6 MeV with no evidence of the piling-up effect.

The leader of stroke 3, besides causing the TGF during its in-cloud development, also produced x-ray pulses characteristic of the stepping process near ground. The pattern of the x-ray-pulse sequence associated with leader stepping near ground was very different from that of the TGF. Specifically, the 15 leader-step pulses that occurred over about 700 μs were separated by time intervals ranging from 6.6 to 177 μs (mean = 47 μs) and tended to increase in amplitude as the leader was approaching the ground (moving into the increasing electric field region). In contrast, the TGF was a compact (35 μs) burst with interpulse intervals ranging from 0.9 to 7.7 μs (mean = 1.9 μs) and pulse amplitudes showing an increasing trend followed by an irregular variation. This disparity supports our view that the TGF was not associated with the leader stepping process, but rather with the negative in-cloud leader entering the upper part of a warmer channel to ground created by the preceding stroke and encountering a relatively sharp air-density gradient (probably related to the relative age of the residual channels of stroke 1 (22 ms) and stroke 2 (10 ms)) there.

Table 2 compares the various scenarios of acceleration and multiplication of runaway electrons in terms of the source of seed electrons, air temperature, and characteristic electric field. Conventional (non-relativistic) avalanches are additionally included as a reference. In table 2, the ambient electron-energy distribution includes electrons with energies less than 30 eV or so, while the so-called cosmic-ray secondaries (electrons produced by very high energy (10^{15}–10^{16} eV or greater) cosmic-ray particles) have energies exceeding 0.1–1 MeV. For comparison, the average energy of electrons in conventional electric breakdown is just a few electron-volts. It follows from table 2 that there are three main factors that can serve to initiate and sustain the acceleration and multiplication of runaway electrons: (1) super-high electric field (row 1), (2) energetic electrons supplied by external sources (row 2), and (3) elevated air temperature (row 3). We suggest that the TGF presented here resulted from the elevated-temperature scenario, previously considered by Mallick *et al* (2012) and Tran *et al* (2015, 2019). In this scenario, runaway electrons giving rise to x-ray/gamma-ray emissions are produced in previously created but decayed channels/branches. Such channels are characterized by elevated temperature of about 3000 K vs 300 K for ambient air, which significantly lowers the friction curve (representing the spatial rate of electron energy loss) relative to that for cold air. As a result, ambient electrons can be accelerated to relativistic speeds in the electric field which is an order of magnitude lower than that required for cold air (compare rows 1 and 3 in table 2). More details are found in Kereszy *et al*

(2022) and Rakov and Kereszy (2022). Note that subsequent-stroke leaders are known to be capable of producing short *E*-field pulses whose peaks satisfy the $\gtrsim$3 MV m^{-1} criterion for the elevated temperature scenario (row 3 in table 2).

TGFs observed to date at ground level in Florida (a total of five) all occurred well after the flash initiation processes. In contrast, Belz *et al* (2020), from recent ground-based observations at 1.4 km above sea level in Utah, reported TGFs associated with the PB process, when there was undisturbed (cold) air between the cloud base and ground. TGFs recorded at ground level in a similar context during winter thunderstorms in Japan were reported by Wada *et al* (2019a, 2020) and Hisadomi *et al* (2021). The lack of observations of TGFs associated with the PB process in Florida could be related to the larger altitude of lightning initiation above the sea-level terrain in Florida compared to the 1.4 km elevated terrain in Utah and to low-altitude winter thunderclouds in Japan. It is not clear why no TGFs occurring well after the cloud-to-ground lightning initiation process; that is, when there exists a strong or weak (residual) electric connection to ground, were reported from the studies in Utah and Japan. Further research is needed to better understand the lightning processes giving rise to TGFs recorded at ground level.

7. Summary

(a) For high-intensity ($\geqslant$50 kA) negative lightning, we found that (a) the PB–RS interval decreases with increasing RS peak current and (b) the range-normalized PB pulse peak increases with the RS peak current. Thus, it appears that the high-intensity negative lightning is characterized by both shorter (and, by inference, faster) stepped leaders and more pronounced (higher-amplitude) PB pulse trains. While it is logical to expect a faster leader to be followed by a more intense RS, it is not clear why the RS intensity is correlated with the intensity of PB which is an in-cloud process. Further research of the PB process (whose current can be comparable to that of RS) and its relation to other lightning processes is needed.

(b) For the first time, complete evolution of a bidirectional leader from its initiation at an altitude of about 4 km to its ground attachment, was optically observed. While the negative-end behavior was normal, the positive end (usually hidden inside the cloud) most of the time appeared to be inactive or showed intermittent luminosity enhancements. Based on a simple electrostatic model, electrical parameters, including the magnitude of charge deposited on either positive or negative part of the bidirectional leader channel and the variation of line charge density along the channel, were estimated.

(c) From high-speed optical imaging, we found that a heavily-branched negative stepped leader creates a highly-structured and rapidly-changing electric field pattern inside and in the vicinity of the volume it occupies, which causes complex interactions between the branches. A negative stepped leader branch tip can collide with the lateral surface of an adjacent (leading) branch, usually at an angle of about 90°. Such generally unexpected collisions are likely to be caused by the attracting Coulomb force of the upward-moving positive charge wave (resembling a mini-RS) associated with stepping of the leading branch.

(d) CIDs are large (hundreds of meters) streamer formations, which, we suggest, are likely to host relatively small hot segments (created, for example, via the thermal ionizational instability) embedded in the overall cold streamer structure. Most of CIDs do not initiate full-fledged flashes and more than half of them exhibit pronounced ringing in their bipolar electric field waveforms, which is indicative of a bouncing-wave process.

(e) TGFs observed at ground level in Florida (a total of five to date) occurred either in the presence of steady current carrying negative charge to ground or during the initial stage of a subsequent-stroke leader; that is, well after the flash-initiation (PB) process. In the presence of full-fledged lightning discharges, runaway electrons giving rise to x-ray/gamma-ray emissions can be produced in previously created but decayed channels/branches. Such channels/branches are non-luminous but are still at an elevated temperature of about 3000 K vs 300 K for ambient air, which significantly lowers the friction curve relative to that for cold air. As a result, ambient electrons can be accelerated to relativistic speeds in the electric field that is an order of magnitude lower than the field required for cold air.

Acknowledgments

This work was supported in part by NSF Grants AGS-2055178 and AGS-2114471. Three Reviewers provided useful comments on the paper.

Data availability statement

No new data were created or analysed in this study.

ORCID iDs

V A Rakov https://orcid.org/0000-0002-4582-9483
M D Tran https://orcid.org/0000-0003-1051-2408
Y Zhu https://orcid.org/0000-0002-9359-4965
Z Ding https://orcid.org/0000-0003-0970-5691
A F R Leal https://orcid.org/0000-0003-0606-2950
I Kereszy https://orcid.org/0000-0001-9855-8608
S Chen https://orcid.org/0000-0002-3575-4035

References

Attanasio A, da Silva C and Krehbiel P 2021 *J. Geophys. Res.: Atmos.* **126** e2021JD034829
Azlinda Ahmad N, Fernando M, Baharudin Z A, Cooray V, Ahmad H and Abdul Malek Z 2010 *J. Atmos. Sol.-Terr. Phys.* **72** 534–40
Belz J W *et al* 2020 *J. Geophys. Res.: Atmos.* **125** e2019JD031940

Berger K 1972 *Bull. Schweiz. Elektrotech. Ver.* **63** 1403–22
Briggs M S *et al* 2010 *J. Geophys. Res.* **115** A07323
Campos L Z S, Saba M M F, Warner T A, Pinto O, Krider E P and Orville R E 2014 *Atmos. Res.* **135–136** 285–305
Chou J-K, Hsu R-R, Su H-T, Chen A B-C, Kuo C-L, Huang S-M, Chang S-C, Peng K-M and Wu Y-J 2018 *J. Geophys. Res. Space Phys.* **123** 3063–77
Cooray V, Cooray G, Marshall T, Arabshahi S, Dwyer J and Rassoul H 2014 *Atmos. Res.* **149** 346–58
Ding Z and Rakov V A 2022 *Electr. Power Syst. Res.* **209** 108043
Ding Z, Rakov V A, Zhu Y, Tran M D, Kostinskiy A Y and Kereszy I 2021 *Geophys. Res. Lett.* **48** e2021GL093295
Dwyer J R *et al* 2004a *Geophys. Res. Lett.* **31** L05118
Dwyer J R *et al* 2004b *Geophys. Res. Lett.* **31** L05119
Dwyer J R, Schaal M M, Cramer E, Arabshahi S, Liu N, Rassoul H K, Hill J D, Jordan D M and Uman M A 2012 *J. Geophys. Res.* **117** A10303
Eack K B 2004 *Geophys. Res. Lett.* **31** L20102
Fishman G J *et al* 1994 *Science* **264** 1313–6
Hare B M *et al* 2016 *J. Geophys. Res.: Atmos.* **121** 6511–33
Hisadomi S *et al* 2021 *J. Geophys. Res.: Atmos.* **126** e2021JD034543
Huang A, Cummer S A and Pu Y 2021 *Geophys. Res. Lett.* **48** e2020GL091553
Iudin D I, Rakov V A, Syssoev A A, Bulatov A A and Hayakawa M 2021 *Sci. Rep.* **11** 18016
Jacobson A R, Light T E L, Hamlin T and Nemzek R 2013 *Ann. Geophys.* **31** 563–80
Karunarathne S, Marshall T C, Stolzenburg M and Karunarathna N 2015 *J. Geophys. Res.: Atmos.* **120** 7128–43
Karunarathne S, Marshall T C, Stolzenburg M and Karunarathna N 2016 *J. Geophys. Res.: Atmos.* **121** 174
Kereszy I, Rakov V A, Ding Z and Dwyer J R 2022 *J. Geophys. Res.: Atmos.* **127** e2021JD036130
Kolmašova I, Santolik O, Farges T, Rison W, Lan R and Uhlíř L 2014 *Geophys. Res. Lett.* **41** 5316–24
Kostinskiy A Y, Bogatov N A, Syssoev V S, Mareev E A, Andreev M G, Bulatov M U, Sukharevsky D I and Rakov V A 2022
Kostinskiy A Y, Marshall T C and Stolzenburg M 2020 *J. Geophys. Res.: Atmos.* **125** e2020JD033191
Kostinskiy A Y, Syssoev V S, Bogatov N A, Mareev E A, Andreev M G, Makalsky L M, Sukharevsky D I and Rakov V A 2015 *Geophys. Res. Lett.* **42** 8165–71
Kotovsky D A *et al* 2016 *J. Geophys. Res. Space Phys.* **121** 5794–804
Krehbiel P R, Riousset J A, Pasko V P, Thomas R J, Rison W, Stanley M A and Edens H E 2008 *Nat. Geosci.* **1** 233–7
Krehbiel P, da Silva C and Cummer S 2018 Continued mysteries of lightning studies *16th Int. Conf. Atmospheric Electricity* (Nara, Japan)
Le Vine D M 1980 *J. Geophys. Res.* **85** 4091
Leal A F R, Rakov V A and Rocha B R P 2019 *Electr. Power Syst. Res.* **173** 251–62
Leal A and Rakov V A 2019 *Sci. Rep.* **9** 12218
Li D *et al* 2021 *J. Geophys. Res.: Atmos.* **126** e2020JA028978
Li D, Luque A, Gordillo-Vazquez F J, da Silva C, Krehbiel P R, Rachidi F and Rubinstein M 2022 *Geophys. Res. Lett.* **49** e2021GL097452
Light T E L 2020 *J. Geophys. Res.: Atmos.* **125** e2019JD032264
Liu F *et al* 2018 *Geophys. Res. Lett.* **45** 2842–51
Liu F *et al* 2021 *Nat. Commun.* **12** 6631
Liu F *et al* 2022 *Ionospheric Elves Powered by Corona Discharges in Overshooting Thunderclouds*
Liu H, Dong W, Wu T, Zheng D and Zhang Y 2012 *J. Geophys. Res.* **117** D01203
Liu N, Spiva N, Dwyer J R, Rassoul H K, Free D and Cummer S A 2015 *Nat. Commun.* **6** 5995
Lü F *et al* 2013 *J. Geophys. Res. Atmos.* **118** 4458–65
Lu G *et al* 2011 *Geophys. Res. Lett.* **38** L12801
Lyu F, Cummer S A, Qin Z and Chen M 2019 *J. Geophys. Res.: Atmos.* **124** 2994–3004
Mallick S, Rakov V A and Dwyer J R 2012 *J. Geophys. Res.* **117** D16107
Marshall T, Bandara S, Karunarathne N, Karunarathne S , Kolmasova I, Siedlecki R and Stolzenburg M 2019 *Atmos. Res.* **217** 10–23
Nag A and Cummins K L 2017 *Geophys. Res. Lett.* **44** 1973–80
Nag A, DeCarlo B A and Rakov V A 2009 *Atmos. Res.* **91** 316–25
Nag A and Rakov V A 2008 *J. Geophys. Res.* **113** D01102
Nag A and Rakov V A 2009 *Geophys. Res. Lett.* **36** L05815
Nag A and Rakov V A 2010a *J. Geophys. Res. Atmos.* **115** D14115
Nag A and Rakov V A 2016 *J. Geophys. Res. Atmos.* **121** 2188–204
Nag A, Rakov V A, Tsalikis D and Cramer J A 2010 *J. Geophys. Res.* **115** D14115
Neubert T *et al* 2020 *Science* **367** 183–6
Neubert T, Chanrion O, Heumesser M, Dimitriadou K, Husbjerg L, Rasmussen I L, Østgaard N and Reglero V 2021 *Nature* **589** 371–5
Raizer Y P 1997 *Gas Discharge Physics* (Berlin: Springer) p 449
Raizer Y P 2009 *Physics of Gas Discharge* (Dolgoprudny: Intellect) p 734
Rakov V A, Mallick S, Nag A and Somu V B 2014 *Electr. Power Syst. Res.* **113** 95–103
Rakov V A, Mareev E A, Tran M D, Zhu Y, Bogatov N A, Kostinskiy A Y, Syssoev V S and Lyu W 2018 *IEEJ Trans. PE* **138** 321–6
Rakov V A 2005 Lightning flashes transporting both negative and positive charges to ground *Recent Progresses in Lightning Physics* ed C Pontikis (Research Signpost) pp 9–21
Rakov V A and Kereszy I 2022 *Electr. Power Syst. Res.* **213** 108736
Rakov V A and Uman M A 2003 *Lightning: Physics and Effects* (Cambridge: Cambridge University Press)
Rison W, Krehbiel P R, Stock M G, Edens H E, Shao X-M, Thomas R J, Stanley M A and Zhang Y 2016 *Nat. Commun.* **7** 10721
Sharma S R, Fernando M and Cooray V 2008 *J. Atmos. Sol.-Terr. Phys.* **70** 1251–60
Shi D, Wang D, Wu T and Takagi N 2019 *J. Geophys. Res.: Atmos.* **124** 8501–10
Smith D A, Shao X M, Holden D N, Rhodes C T, Brook M, Krehbiel P R, Stanley M, Rison W and Thomas R J 1999 *J. Geophys. Res.* **104** 4189–212
Smith D M, Lopez L I, Lin R P and Barrington-Leigh C P 2005 *Science* **307** 1085–8
Soler S *et al* 2020 *J. Geophys. Res.: Atmos.* **125** e2020JD032708
Stolzenburg M, Marshall T C, Bandara S, Hurley B and Siedlecki R 2021 *Meteorol. Atmos. Phys.* **133** 1177–202
Syssoev A A, Iudin D I, Bulatov A A and Rakov V A 2020 *J. Geophys. Res. Atmos.* **125** e2019JD031360
Tilles J N, Liu N, Stanley M A, Krehbiel P R, Rison W, Stock M G, Dwyer J R, Brown R and Wilson J 2019 *Nat. Commun.* **10** 1648
Tran M D, Kereszy I, Rakov V A and Dwyer J R 2019 *Geophys. Res. Lett.* **46** 9252–60
Tran M D and Rakov V A 2016 *Sci. Rep.* **6** 39521
Tran M D, Rakov V A, Mallick S, Dwyer J R, Nag A and Heckman S 2015 *J. Atmos. Sol.-Terr. Phys.* **136** 86–93
Wada Y *et al* 2019a *Commun. Phys.* **2** 67
Wada Y *et al* 2020 *J. Geophys. Res.: Atmos.* **125** e2019JD031730
Wang D, Takagi N, Watanabe T, Rakov V A and Uman M A 1999 *J. Geophys. Res.* **104** 14369–76
Willett J C, Bailey J C and Krider E P 1989 *J. Geophys. Res.* **94** 16255
Wu T, Dong W, Zhang Y, Funaki T, Yoshida S, Morimoto T, Ushio T and Kawasaki Z 2012 *J. Geophys. Res.* **117** D05119

Wu T, Dong W, Zhang Y and Wang T 2011 *J. Geophys. Res.* **116** D03111

Wu T, Takayanagi Y, Yoshida S, Funaki T, Ushio T and Kawasaki Z 2013 *Geophys. Res. Lett.* **40** 618–23

Zhu B, Zhou H, Ma M and Tao S 2010 *J. Atmos. Sol.-Terr. Phys.* **72** 271–8

Zhu Y, Rakov V A, Mallick S, Tran M D, Pilkey J and Uman M A 2014 Preliminary breakdown pulse trains in electric field records of negative cloud to ground lightning *15th Int. Conference on Atmos. Electricity* (Norman, Oklahoma, U.S.A. 15–20 June 2014) p 9

Zhu Y, Rakov V A and Tran M D 2016 *Atmosphere* **7** 130